Research Square

Preprints are preliminary reports that have not undergone peer review.
They should not be considered conclusive, used to inform clinical practice,
or referenced by the media as validated information.

Femoral Surface Stress Redistribution After Cemented Stem Insertion With Distal Lateral Stress Concentration in an Osteoporotic Composite Femur Model

Shota Yasunaga

syasunaga@tsukuba-seikei.jp

University of Tsukuba

Ryunosuke Watanabe

University of Tsukuba

Tomohiro Yoshizawa

University of Tsukuba

Hajime Mishima

Tsukuba Central Hospital

Yasuhiro Homma

University of Tsukuba

Yoshihisa Harada

National Institute of Advanced Industrial Science and Technology

Research Article

Keywords: Total hip arthroplasty, Osteoporosis, Thermoelastic stress analysis, Load transfer

Posted Date: November 23rd, 2026

DOI: https://doi.org/10.21203/rs.3.rs-11672958/v1

License: This work is licensed under a Creative Commons Attribution 4.0 International License.
Read Full License

Additional Declarations: No competing interests reported.

Title

Femoral Surface Stress Redistribution After Cemented Stem Insertion With Distal Lateral Stress Concentration in an Osteoporotic Composite Femur Model

Abstract

Introduction

Previous thermoelastic studies have shown that cemented stem implantation shifts femoral stress distally, but regional averages provide limited information about the location of individual stress peaks. This study aimed to characterize femoral surface stress redistribution after implantation of the Trilliance polished taper-slip cemented stem in normal and osteoporotic composite femora.

Materials and Methods

Three normal and three osteoporotic composite femora were tested before and after stem implantation. Size 10 and size 16 high-offset stems were used in the normal and osteoporotic models, respectively. Cyclic compressive loads of 100–1900 N and 100–1000 N, respectively, were applied at 5 Hz. Thermoelastic stress analysis measured changes in the sum of the surface principal stresses. Longitudinal stress profiles along the medial and lateral surfaces were evaluated descriptively. For each implanted specimen, the location of peak lateral stress was recorded relative to the stem tip.

Results

In both models, proximal surface stress decreased after implantation, and the peaks of the mean medial and

lateral stress profiles shifted distally. In the normal model, distal stress changed little, and individual lateral peaks were located 50–82 mm proximal to the stem tip. In the osteoporotic model, distal stress increased on both surfaces. All three lateral peaks were within 16 mm of the stem tip, including one 16 mm distal to the tip.

Conclusions

Under the conditions tested, the osteoporotic specimens showed increased distal surface stress after implantation, with the lateral stress peak consistently located near the stem tip. Differences in stem size and loading conditions precluded attribution of this pattern to bone properties alone.

Keywords: Total hip arthroplasty; Osteoporosis; Thermoelastic stress analysis; Load transfer

Introduction

The fixation method and design of femoral stems substantially influence postoperative load transfer and femoral stress distribution following total hip arthroplasty (THA) [1]. These mechanical changes may affect postoperative bone remodeling and are associated with complications such as periprosthetic femoral fracture and implant loosening [2–4].

Osteoporosis is common among patients awaiting joint arthroplasty [5], including those scheduled for THA [6]. In patients undergoing THA, low bone mineral density is a clinical concern because of its association with periprosthetic fracture [7]. In patients aged 65 years or older undergoing THA, cemented femoral fixation has been associated with a lower risk of periprosthetic fracture than cementless fixation [8,9]. Consequently, understanding load transfer and stress distribution after cemented THA in osteoporotic bone is important for preventing postoperative complications and optimizing implant design.

Thermoelastic stress analysis (TSA) is a noncontact full-field technique that measures minute temperature changes associated with elastic deformation using an infrared camera, thereby enabling visualization of surface stress distribution [10]. In the field of THA, TSA has been used to evaluate femoral surface stress distribution and to investigate the effects of stem design and fixation method on load transfer [11]. A recent TSA study comparing cementless and cemented stems with identical geometry demonstrated that cemented fixation reduced proximal femoral stress and shifted stress distribution distally, further illustrating the influence of fixation method on femoral load transfer [12]. Furthermore, a previous TSA study comparing normal and osteoporotic composite femora demonstrated that stress redistribution following cemented

stem implantation was greater in the osteoporotic model, with a distal shift in stress distribution and the highest stress observed around the stem tip [13]. Thus, proximal stress reduction and distal stress redistribution following cemented stem implantation have already been demonstrated in previous TSA studies. However, previous studies have evaluated only a limited number of polished taper-slip cemented stem designs, and stress redistribution with stems of different geometries remains incompletely understood. Therefore, this study aimed to characterize changes in femoral surface stress distribution after implantation of the Trilliance polished taper-slip cemented stem in normal and osteoporotic composite femora.

Materials

Composite femora

Two types of composite femora with different bone qualities were used in this study (Fig. 1). Composite Femur #3403 (Sawbones; Pacific Research Laboratories, Vashon, WA, USA), which represents an adult male femur, was used as the normal bone model. This model reproduces the geometry of an adult male cadaveric femur and consists of a cortical shell made of short glass fiber-reinforced epoxy and cancellous bone made of polyurethane foam with a density of 17 pcf (approximately 0.27 g/cm^3). The intramedullary canal structure is also reproduced, and the model has been reported to exhibit less interspecimen mechanical variability than cadaveric bone [14,15].



Fig. 1 Composite Femur #3403 representing a normal adult male femur (a) and Composite Femur #3503 representing an osteoporotic femur (b). Axial CT images are shown in the upper right corner of each panel.

Both models have identical external geometry; however, the osteoporotic model demonstrates a thinner cortical shell and a larger medullary canal.

Composite Femur #3503 (Sawbones; Pacific Research Laboratories, Vashon, WA, USA), which represents an osteoporotic femur, was used as the osteoporotic bone model. This model has the same external geometry as the normal bone model but features a thinner cortical shell and cancellous bone composed of polyurethane foam with a density of 10 pcf (0.16 g/cm³). Mechanical testing using osteoporotic cadaveric femora has demonstrated that this model reproduces the mechanical response of osteoporotic bone [16].

Stem and head

The Trilliance Stem (Aesculap, B. Braun, Melsungen, Germany) was used. This cobalt–chromium cemented stem is a polished taper-slip design with a triple-taper geometry and is intended for line-to-line implantation [17]. Stem size and implantation were planned using three-dimensional implantation planning software (ZedHip, version 17.0.0; Lexi Co., Ltd., Tokyo, Japan) to reproduce the position of the femoral head apex (Fig. 2).

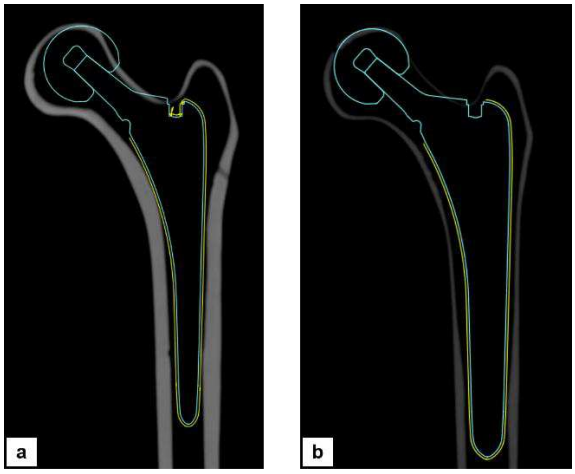


Fig. 2 Three-dimensional implantation planning was performed using ZedHip software (version 17.0.0) to reproduce the position of the femoral head apex. A #10 High Offset stem was selected for the normal bone model (a), whereas a #16 High Offset stem was selected for the osteoporotic bone model (b).

The femoral neck osteotomy was set 15 mm proximal to the lesser trochanter on the medial side and at an angle of 135° relative to the femoral shaft axis. Stem alignment was standardized at neutral varus–valgus alignment, 2° of flexion, and 10° of anteversion. A #10 High Offset stem was used in the normal bone model, whereas a #16 High Offset stem was used in the osteoporotic bone model. A 32-mm BIOLOX® DELTA TS femoral head was used, and PALACOS bone cement (Heraeus Medical, Wehrheim, Germany) was used for stem fixation.

Methods

Thermoelastic stress analysis

Thermoelastic stress analysis (TSA) was used for mechanical evaluation in this study. TSA is a noncontact technique for assessing surface stress distributions based on minute temperature changes generated when a material undergoes adiabatic elastic deformation, known as the thermoelastic effect. The thermoelastic effect was first described by Thomson [18]and is expressed by the following equation:

$$\Delta T = -kT\Delta(\sigma_1 + \sigma_2)$$

where ΔT is the temperature change (K), k is the thermoelastic coefficient (Pa^{-1}), T is the absolute temperature (K), and $\Delta(\sigma_1 + \sigma_2)$ is the change in the sum of the principal stresses (Pa).

Hyodo et al. developed a TSA-based system for analyzing surface stress distributions in composite femora after stem implantation and demonstrated its utility [11]. The thermoelastic properties of the short glass fiber-reinforced epoxy used in the composite femora in the present study have also been reported. A temperature change of 1 K corresponds to a change of approximately 227 MPa in the sum of the principal stresses, with a thermoelastic coefficient of 1.47×10^{-11} Pa^{-1} [11]. In this study, the reported stress values represent the change in the sum of the surface principal stresses during cyclic loading. Negative values indicate a compressive change in the sum of the principal stresses, and positive values indicate a tensile change. Reductions in stress refer to decreases in the magnitude of this change.

Specimen preparation and measurement protocol

Three composite femora were used for each of the normal and osteoporotic models, consistent with the sample size used in previous TSA studies employing composite femora [12,13]. Specimen preparation,

loading conditions, and TSA image acquisition followed the protocol described in the previous study [13]. All six specimens were distinct from those used in the previous study, and preimplantation TSA data were acquired separately for each specimen in the present study. Specimen preparation was performed by two hip surgeons experienced in THA procedures. After resection of the distal portion of each composite femur, the specimen was fixed in a holder at 9° of valgus and 2° of flexion to simulate single-leg stance. To ensure uniform surface emissivity, the surface of each composite femur was uniformly coated with matte black heat-resistant paint (Asahipen Corporation, Osaka, Japan). The specimens in this condition, before stem implantation, were designated as the control groups: the control N group for the normal model and the control O group for the osteoporotic model (Fig. 3a).

Each composite femur was mounted on a servohydraulic testing machine (MTS 858 Mini Bionix; MTS Systems Corporation, Eden Prairie, MN, USA), and cyclic vertical compressive loading was applied to the apex of the femoral head using a sinusoidal waveform at 5 Hz. For the normal model, the load ranged from 100 to 1900 N. The maximum load corresponded to approximately twice the estimated body weight represented by Composite Femur #3403, approximately 890 N, and was selected to simulate the hip joint load during the single-leg stance phase of level walking [19]. For the osteoporotic model, the maximum load was set at 1000 N, approximately twice the average body weight of elderly Japanese women, 51.0 kg or approximately 500 N, and the applied load ranged from 100 to 1000 N [20].

After stabilization of the applied load, infrared images over 100 loading cycles were acquired using an infrared stress measurement system (CPA-SC7500; FLIR Systems Inc., Wilsonville, OR, USA) (Fig. 4).

The acquired images were synchronized with the applied load and processed using analysis software (Altair, version 5.91.010; FLIR Systems Inc.). Surface stress distribution images of the femur were obtained from four views: anterior, posterior, medial, and lateral (Fig. 5).

Stem implantation was subsequently performed in the same specimens. Femoral neck osteotomy and preparation of the medullary canal were performed according to the preoperative plan. Under fluoroscopic guidance, a cement restrictor was placed 1 cm distal to the stem tip. After vacuum mixing, the bone cement was injected retrogradely using a cement gun, followed by insertion of the Trilliance Stem. The specimens were then recoated with matte black heat-resistant paint and designated as the stem-implanted groups: the insert N group for the normal model and the insert O group for the osteoporotic model (Fig. 3b). TSA was repeated after stem implantation under the same loading conditions, and surface stress distribution images were acquired.

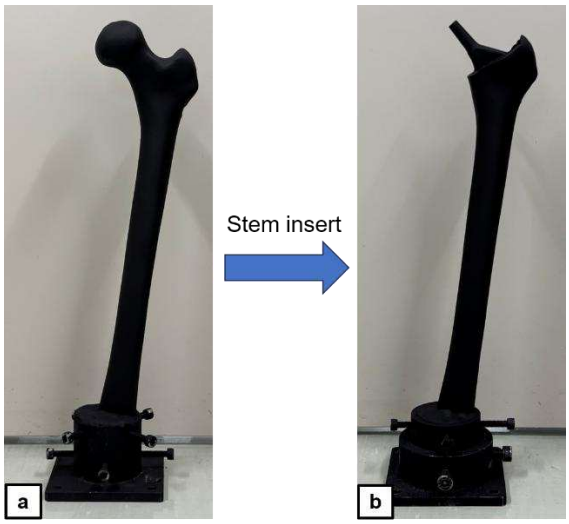


Fig. 3 Composite femur before stem implantation (control group, a) and after stem implantation (insert

group, b). The stem was implanted in neutral varus–valgus alignment with 2° of flexion and 10° of anteversion.

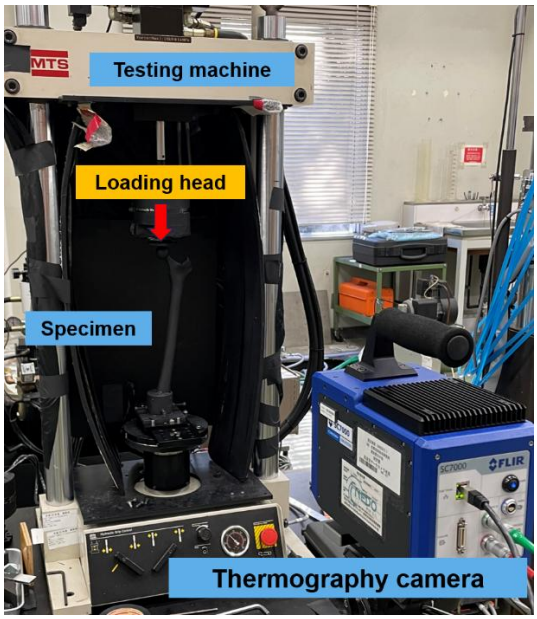


Fig. 4 The composite femur was mounted on a servohydraulic testing machine (MTS 858 Mini Bionix), and cyclic compressive loading was applied to the apex of the femoral head. Thermoelastic stress analysis was performed using a high-sensitivity infrared camera (CPA-SC7500).

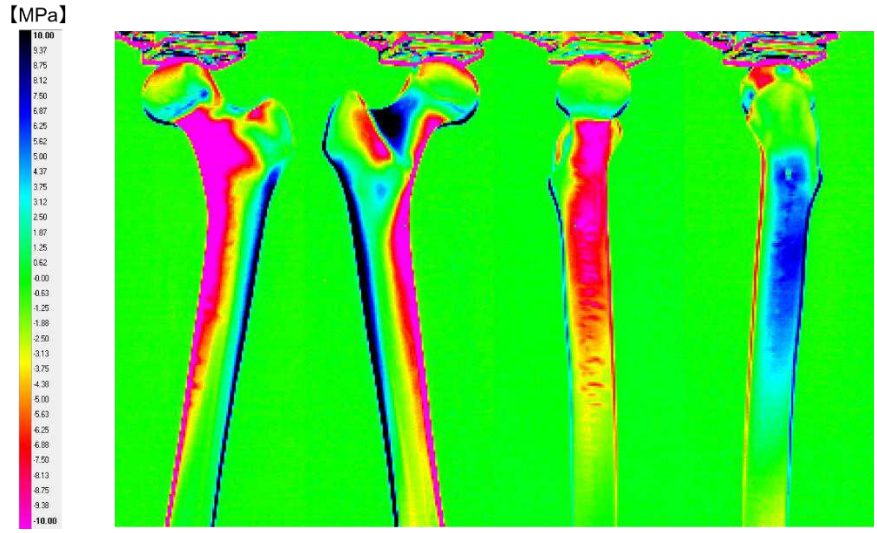


Fig. 5 Surface stress distribution images were acquired from four aspects of the femur: anterior, lateral, posterior, and medial. Red indicates compressive stress, whereas blue indicates tensile stress.

Outcome assessment

Qualitative assessment

Surface stress distribution images of the medial and lateral aspects of the composite femora were visually assessed in each group. Within each bone model, the same color scale was used for the stress maps before and after stem implantation. The locations of stress concentration and changes in stress distribution patterns were compared between the control and stem-implanted groups.

Quantitative line analysis

Quantitative line analysis was performed on the medial and lateral aspects of the composite femora, corresponding to the regions evaluated qualitatively. On both the medial and lateral surfaces, a one-pixel-

wide measurement line was positioned midway between the anterior and posterior aspects of the femur and parallel to the longitudinal axis of the femoral shaft (Fig. 6). The sum of the principal stresses was measured continuously along each line to evaluate stress distribution in the longitudinal direction of the femur. Gruen zones [21]were used as anatomical landmarks for the measurement locations.

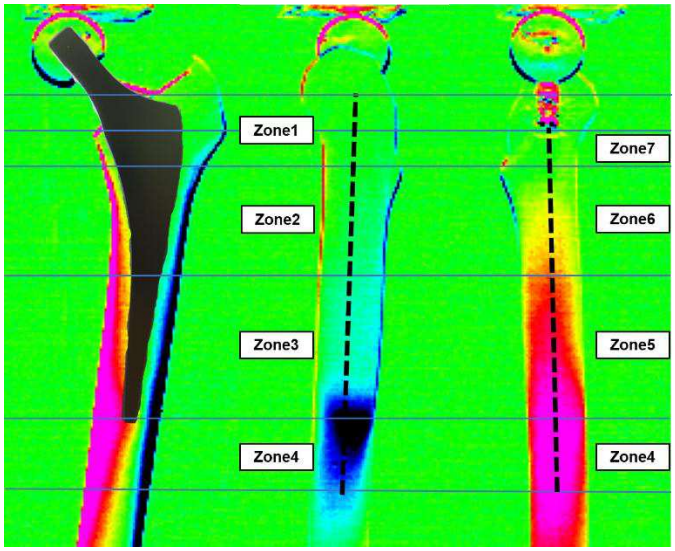


Fig. 6 Dashed lines indicate the measurement lines positioned on the medial and lateral femoral surfaces, parallel to the longitudinal axis of the femur and midway between the anterior and posterior aspects. The sum of the principal stresses was continuously measured along each line to evaluate its longitudinal distribution. Gruen zones were used as anatomical references for measurement locations.

Within each bone model, the measurement lines were aligned at their starting points, and stress values at the same distance from the starting point were averaged across the three specimens. The resulting mean

profiles were compared before and after stem implantation. In addition, the peak value of the mean stress distribution and its corresponding location were determined for each group. For each implanted specimen, peak lateral stress was defined as the maximum value along the entire lateral measurement line. Its location was recorded by Gruen zone and distance from the stem tip. The stem tip was localized on the stress distribution image by aligning it with the postimplantation fluoroscopic image using the femoral head and the greater and lesser trochanters as landmarks. The known body dimensions of each implanted stem were used to calibrate the image scale and convert the longitudinal distance from the stem tip to the lateral stress peak from pixels to millimeters. To preserve localized features that might be obscured by averaging stress values across Gruen zones, we evaluated the continuous stress profiles before and after implantation in the same three specimens per model. Results are presented descriptively for individual specimens and as group mean profiles. No inferential statistical analyses were performed.

Results

Qualitative assessment

In the normal bone model, the overall color intensity was reduced after stem implantation compared with the control N group, indicating a decrease in stress over the femoral surface (Fig. 7). This reduction was observed on both the medial and lateral aspects and was most pronounced in the proximal region.

In the osteoporotic bone model, the proximal region showed reduced color intensity after stem implantation compared with the control O group, whereas the distal region exhibited increased color intensity (Fig. 8). This tendency was particularly evident on the lateral aspect, where localized stress concentration was observed around the stem tip.

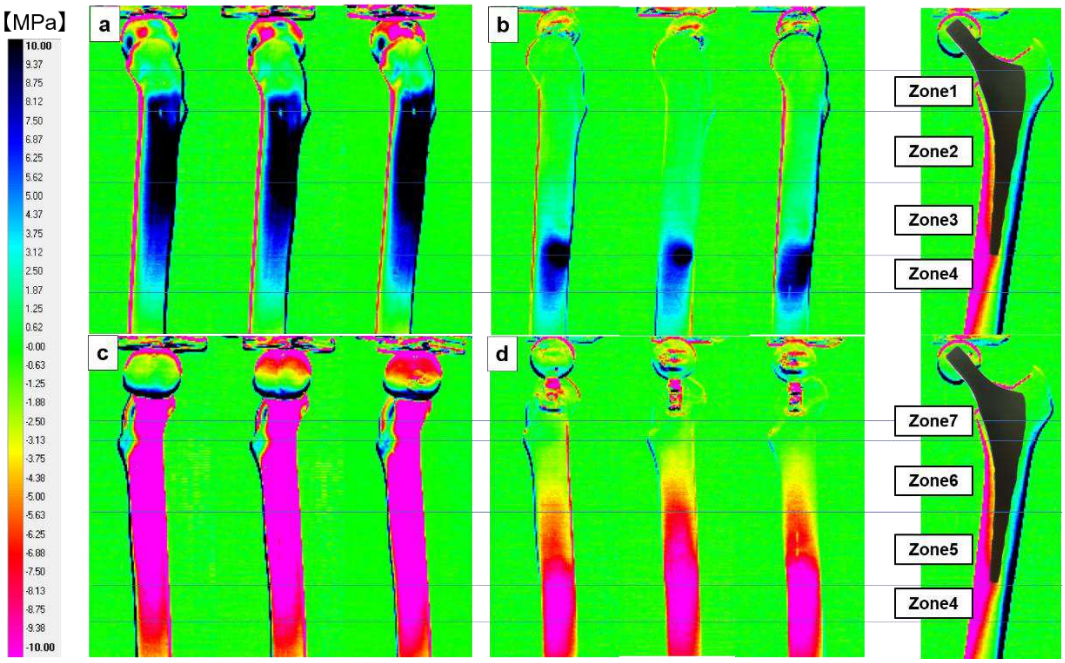


Fig. 7 Thermoelastic stress distribution images of the normal bone model: control N group (a, lateral; c, medial) and insert N group (b, lateral; d, medial). Compared with the control N group, the insert N group

demonstrated an overall reduction in surface stress on both aspects, which was most pronounced proximally.

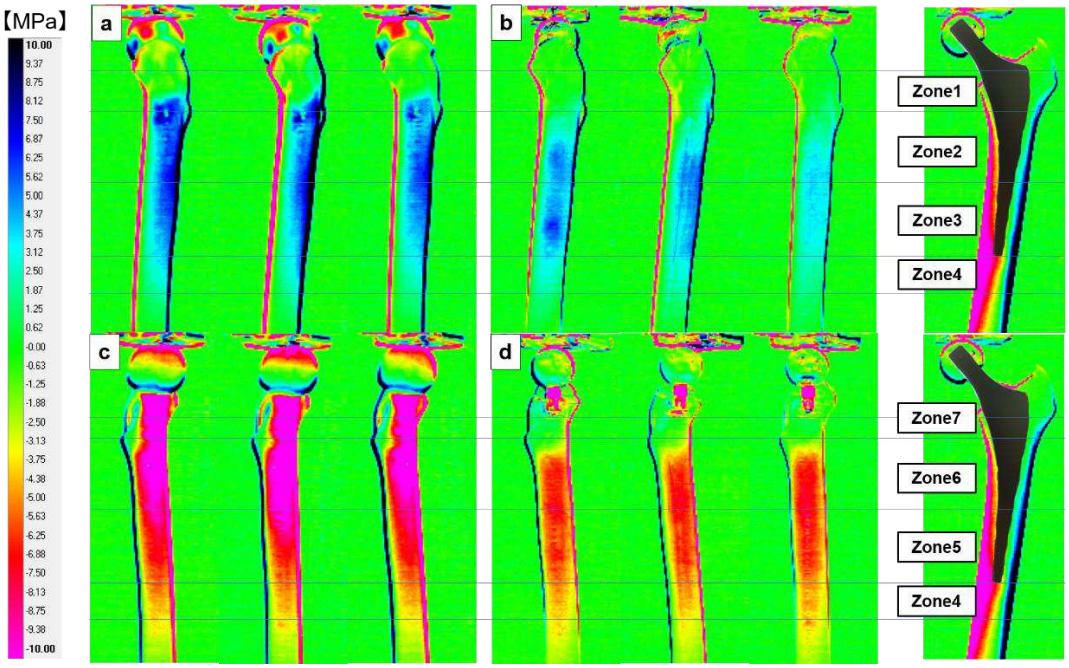


Fig. 8 Thermoelastic stress distribution images of the osteoporotic bone model: control O group (a, lateral; c, medial) and insert O group (b, lateral; d, medial). Compared with the control O group, the insert O group demonstrated reduced proximal surface stress and increased distal surface stress. A localized stress concentration was observed around the stem tip on the distal lateral aspect.

Quantitative line analysis

Stress distributions along the femoral shaft are shown in Figs. 9 and 10, and the peak lateral stress, its corresponding Gruen zone, and the distance from the stem tip to the peak stress location for each specimen

are summarized in Table 1.

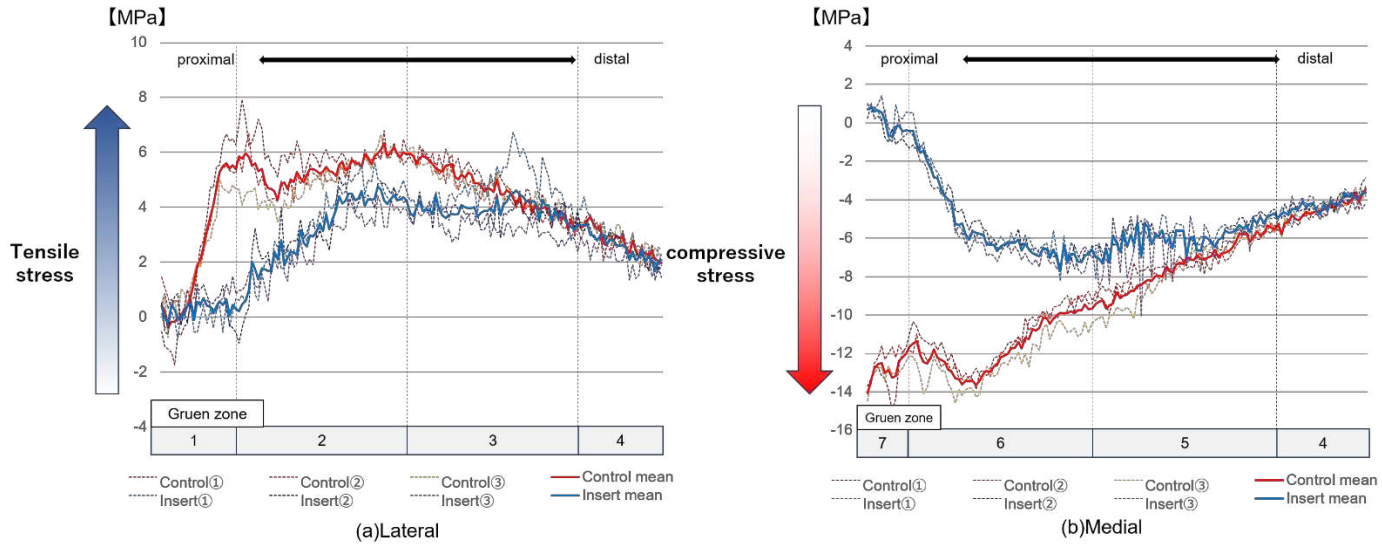


Fig. 9 Longitudinal surface stress distributions in the normal bone model on the lateral (a) and medial (b) aspects. Thin lines represent individual specimens, and thick lines represent group means. Following stem implantation, proximal surface stress decreased and the location of the peak mean stress shifted distally on both aspects, without a marked increase in distal stress.

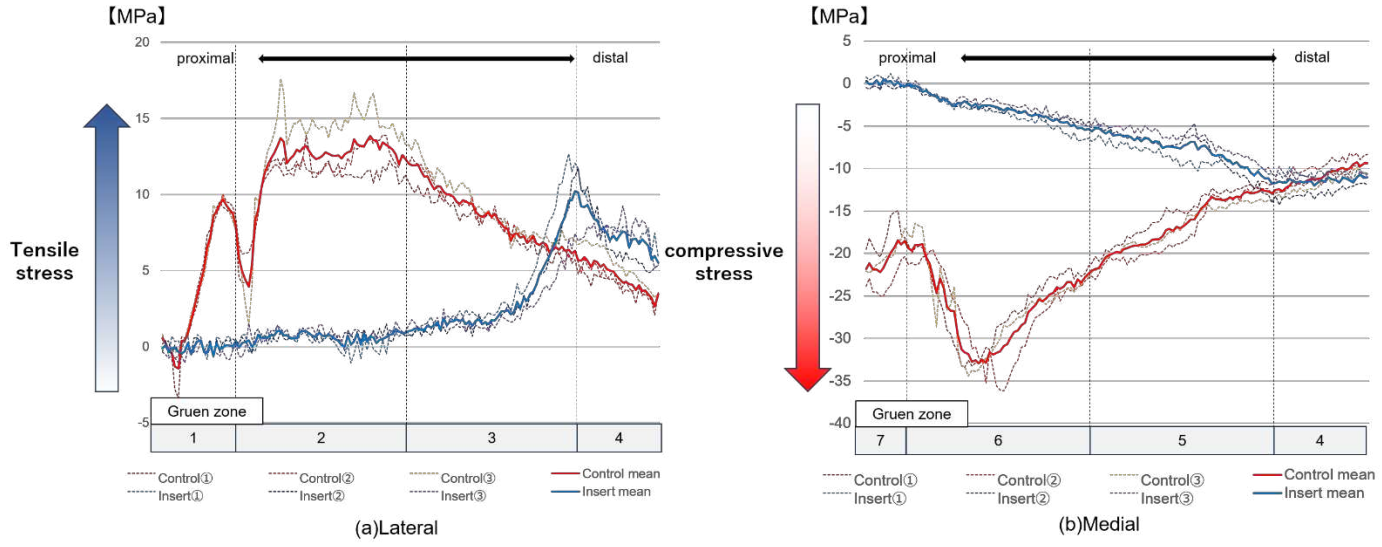


Fig. 10 Longitudinal surface stress distributions in the osteoporotic bone model on the lateral (a) and

medial (b) aspects. Thin lines represent individual specimens, and thick lines represent group means. Following stem implantation, proximal surface stress decreased and distal surface stress increased on both aspects. The peak of the mean stress profile shifted distally on both surfaces. After implantation, the peak of each specimen's lateral stress profile was located within 16 mm of the stem tip.

Table 1 Individual specimen data for the location and magnitude of peak lateral stress following stem implantation

Model	Specimen	Peak location	Distance from stem tip (mm)	Peak lateral stress (MPa)
Normal	1	Zone 3	50	6.7
	2	Zone 2	69	4.9
	3	Zone 2	82	4.6
Osteoporotic	1	Zone 3	4	12.7
	2	Zone 3	0	11.7
	3	Zone 4	−16	9.3

Peak location (Gruen zone), distance from the stem tip, and peak lateral stress are presented for each specimen following stem implantation. Positive values indicate locations proximal to the stem tip, negative values indicate locations distal to the tip, and zero indicates the level of the tip.

In the normal bone model, stem implantation reduced proximal stress, particularly in Gruen zones 2 and 6–7. In the distal region, the stress distributions of the control and stem-implanted groups gradually converged, with little change in distal stress after stem implantation. The location of the peak mean stress

250 shifted distally on both the medial and lateral aspects. In individual specimens, the peak lateral tensile
251 stress after stem implantation ranged from 4.6 to 6.7 MPa and was located in Gruen zone 2 in two
252 specimens and zone 3 in one specimen, at distances of 50–82 mm from the stem tip.
253 In the osteoporotic bone model, stem implantation reduced proximal stress and increased distal stress on
254 both the medial and lateral aspects. On the medial aspect, the stress profiles of the two groups crossed in
255 the proximal portion of Gruen zone 4, whereas on the lateral aspect, the crossover occurred in the distal
256 portion of Gruen zone 3. The location of the peak mean stress shifted distally on both the medial and
257 lateral aspects. After implantation, peak lateral stress ranged from 9.3 to 12.7 MPa and was located in
258 Gruen zone 3 in two specimens and zone 4 in one specimen. All three peaks were within 16 mm of the
259 stem tip, with one peak located 16 mm distal to the tip (Table 1).

Discussion

In this study, thermoelastic stress analysis demonstrated that implantation of a polished taper-slip cemented stem reduced proximal femoral stress and shifted the location of peak stress distally in both the normal and osteoporotic bone models. These findings are consistent with previous TSA studies demonstrating proximal stress reduction and distal stress redistribution following cemented stem implantation [12,13]. However, the pattern of distal stress redistribution differed between the two bone models. In the normal model, distal surface stress changed little after implantation. In the osteoporotic model, distal surface stress increased on both the medial and lateral surfaces, and the lateral stress peak was within 16 mm of the stem tip in all three specimens.

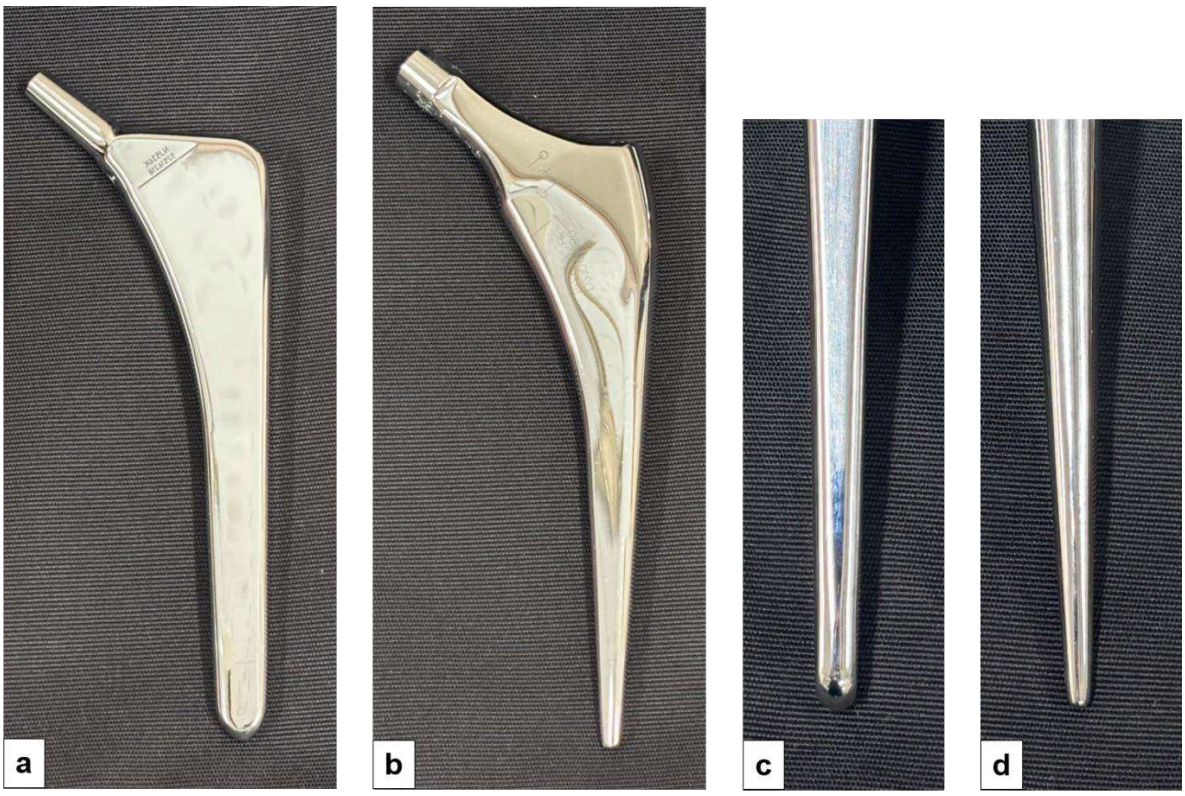
The reduction in proximal stress and distal shift of the peak stress after stem implantation are consistent with previous finite element and experimental studies of cemented stems [1,12,13]. In cemented stems, load is transferred from the implant to the femur through the cement mantle rather than by direct stem–bone contact. Consequently, the mechanical load borne by the proximal femur is reduced, resulting in decreased proximal stress.

The pattern of stress redistribution differed between the two bone models. Similar distal migration of stress and increased peak stress in osteoporotic bone have been reported previously [13]. The distal stress redistribution observed in the osteoporotic model may be related to the thinner cortical bone and the larger stem size used in this model. These factors may increase the proportion of load transmitted through the stem, resulting in greater distal load transfer. A stiffness mismatch between the stem and the surrounding

bone may also have contributed to the localized increase in lateral surface stress near the stem tip. Stem size itself may also have influenced the observed stress redistribution. A recent biomechanical study using the same osteoporotic composite femur model demonstrated that stem sizing influenced torsional periprosthetic fracture resistance after cemented stem implantation [22]. Because stem size and loading conditions also differed between the two models, the independent contribution of bone properties to the observed differences in stress redistribution could not be determined.

The localized distal lateral stress concentration may therefore reflect several interacting factors, including bone quality, distal load transfer, stem size, and stem geometry. Previous studies have shown that stem design influences femoral load transfer and stress distribution [1,11]. In a finite element model with proximal stem–cement bonding, Mann et al. found that stem geometry influenced stress distribution at both the stem–cement and cement–bone interfaces [23]. The C-stem AMT used in a previous TSA study [13], similar to the Trilliance stem used in the present study, is a polished taper-slip stem with a triple-tapered design, including tapering in the mediolateral direction. In the anteroposterior view, the lateral border of the Trilliance stem shows little taper. In the lateral view, the Trilliance stem appears to taper more gradually toward the tip than the C-stem AMT (Fig. 11). In the previous C-stem AMT study, the highest mean stress on the lateral surface after implantation was found in Gruen zone 4L in the osteoporotic model [13]. In the present study, continuous line analysis showed that the lateral stress peak was located within 16 mm of the Trilliance stem tip in all three osteoporotic specimens. The limited lateral taper of the Trilliance stem may have contributed to this peak, although the present study did not isolate the effect of stem

298 geometry. Under the loading conditions used for each model, distal femoral surface stress changed little
299 after stem implantation in the normal model but increased on both the medial and lateral surfaces in the
300 osteoporotic model. Despite these biomechanical findings, excellent long-term clinical outcomes have
301 been reported for the Trilliance stem. Miyamoto et al. reported 100% survivorship with femoral revision
302 for aseptic loosening as the endpoint at a mean follow-up of 10.7 years in 151 hips [24]. This series
303 documents favorable long-term femoral fixation with the Trilliance stem, although the clinical significance
304 of the localized stress peak observed in our model remains unknown.
305



306
307 **Fig. 11** Representative photographs of the Trilliance stem and the C-stem AMT: anteroposterior views of
308 the Trilliance stem (a) and C-stem AMT (b), and lateral views of the Trilliance stem (c) and C-stem AMT

(d). Both stems have a triple-tapered design. However, unlike the C-stem AMT, the Trilliance stem has little taper on the lateral surface in the anteroposterior view. In the lateral view, the Trilliance stem appears to taper more gradually toward the tip than the C-stem AMT.

The localized distal lateral stress concentration, particularly around the stem tip, may also have implications for the pathogenesis of atypical periprosthetic femoral fracture (APFF), a periprosthetic femoral fracture with radiographic features resembling those of atypical femoral fracture (AFF), including a transverse fracture pattern, minimal comminution, and localized thickening of the lateral cortex [25,26]. Among patients aged 65 years or older undergoing THA, cemented femoral fixation has been associated with a lower overall risk of periprosthetic fracture than cementless fixation [8,9]. Nevertheless, atypical periprosthetic femoral fractures have been reported around both cemented and cementless stems [25,27]. In a multicenter study of APFFs around cemented stems, 15 of 20 fractures (75%) occurred around the stem tip, and 13 of the 17 hips with pre-fracture radiographs (76%) showed lateral cortical beaking or flaring [28]. Their pathogenesis is considered multifactorial, involving suppressed bone turnover associated with long-term antiresorptive therapy, femoral geometry, and repetitive mechanical loading of the lateral femoral cortex [26,29]. In a previous TSA study, implantation of a cemented stem in the same osteoporotic composite femur model resulted in distal migration of stress distribution and increased stress around the stem tip [13]. In a CT-based finite element study of AFF, Oh et al. found that the site of maximum tensile

328 stress was close to the fracture site [29]. In the present study, the lateral surface stress peak was located
329 near the stem tip in all three osteoporotic specimens, a region where APFFs around cemented stems
330 frequently occur [28]. Whether this localized stress pattern contributes to APFF remains unknown, as the
331 present study evaluated surface stress under cyclic loading but did not assess fracture initiation or
332 propagation.
333 This study has several limitations. First, only three femora were tested per model. Although the lateral
334 stress peak was located near the stem tip in all three osteoporotic specimens, this small sample provides
335 limited information about variability in peak location across specimens.
336 Second, different loading conditions were applied to the normal and osteoporotic bone models to reflect
337 their respective assumed body sizes. Within each model, the same loading conditions were used before and
338 after implantation, allowing stress redistribution to be assessed within specimens. However, the different
339 load ranges limit direct comparison of stress magnitudes between models.
340 Third, this study evaluated only the immediate postoperative condition and did not account for time-
341 dependent changes such as stem subsidence and subsequent bone remodeling [30], both of which may
342 further influence stress redistribution.
343 Fourth, only one stem design was tested in the present study. Although the previous C-stem AMT study
344 used the same composite femur models, loading conditions, and TSA system [13], the two stems were
345 evaluated in separate experiments. Moreover, the previous study quantified regional mean stress, which
346 limits direct comparison of localized stress peaks between the two studies. In addition, different stem sizes

were selected for the normal and osteoporotic bone models to reproduce clinically appropriate implantation. Therefore, the observed differences in stress redistribution may have been influenced, at least in part, by differences in stem size.

Finally, TSA is well suited for evaluating surface stress distribution but cannot directly assess stress within the femur. Combining TSA with finite element analysis may provide a more comprehensive understanding of femoral stress distribution in future studies.

Despite these limitations, this study provides additional biomechanical information regarding stress redistribution following implantation of a polished taper-slip cemented stem under normal and osteoporotic bone conditions. These findings may contribute to a better understanding of femoral load transfer and provide a biomechanical basis for future implant design and clinical investigations in patients with osteoporosis.

Conclusion

Using thermoelastic stress analysis, this study evaluated changes in femoral surface stress distribution following implantation of a polished taper-slip cemented stem in composite femora with different mechanical properties. Stem implantation reduced proximal femoral stress and shifted the location of peak stress distally in both the normal and osteoporotic bone models. In the osteoporotic model, distal stress redistribution was accompanied by a localized increase in distal lateral stress around the stem tip.

These findings suggest that bone quality influences femoral load transfer following implantation of a polished taper-slip cemented stem. They also suggest that localized stress redistribution is influenced by multiple factors, including stem size and geometry. The present findings provide additional biomechanical insight into femoral load transfer following cemented stem implantation and may serve as a basis for future studies of implant design and postoperative complications in patients with osteoporosis.

References

1. Huiskes R (1990) The various stress patterns of press-fit, ingrown, and cemented femoral stems. Clin Orthop Relat Res 261:27–38.

2. Wan Z, Dorr LD, Woodsome T, Ranawat A, Song M (1999) Effect of stem stiffness and bone stiffness on bone remodeling in cemented total hip replacement. J Arthroplasty 14:149–158. https://doi.org/10.1016/S0883-5403(99)90006-8

3. Fleischman AN, Chen AF (2015) Periprosthetic fractures around the femoral stem: overcoming challenges and avoiding pitfalls. Ann Transl Med 3:234. https://doi.org/10.3978/j.issn.2305-5839.2015.09.32

4. Huiskes R, Weinans H, van Rietbergen B (1992) The relationship between stress shielding and bone resorption around total hip stems and the effects of flexible materials. Clin Orthop Relat Res 274:124–134. https://doi.org/10.1097/00003086-199201000-00014

5. Lingard EA, Mitchell SY, Francis RM, Rawlings D, Peaston R, Birrell FN, McCaskie AW (2010) The prevalence of osteoporosis in patients with severe hip and knee osteoarthritis awaiting joint arthroplasty. Age Ageing 39:234–239. https://doi.org/10.1093/ageing/afp222

6. Watanabe N, Miyatake K, Takada R, Ogawa T, Amano Y, Jinno T, Koga H, Yoshii T, Okawa A (2022) The prevalence and treatment of osteoporosis in patients undergoing total hip arthroplasty and the levels of biochemical markers of bone turnover. Bone Joint Res 11:873–880. https://doi.org/10.1302/2046-3758.1112.BJR-2022-0252.R1

7. Daher M, Mekhael E, El-Othmani MM (2024) Total hip arthroplasty in patients with hip osteoporosis: a narrative review. Hip Pelvis 36:260–272. https://doi.org/10.5371/hp.2024.36.4.260

8. Kelly M, Chen AF, Ryan SP, Working ZM, Porter KR, De A, Mullen K, Kagan R (2023) Cemented femoral fixation in total hip arthroplasty reduces the risk of periprosthetic femur fracture in patients 65 years and older: an analysis from the American Joint Replacement Registry. J Arthroplasty 38(Suppl):S351–S354. https://doi.org/10.1016/j.arth.2023.04.039

9. Hameed D, McCormick BP, Sequeira SB, Dubin JA, Bains SS, Mont MA, Delanois RE, Boucher HR (2024) Cemented versus cementless femoral fixation for total hip arthroplasty following femoral neck fracture in patients aged 65 and older. J Arthroplasty 39:1747–1751. https://doi.org/10.1016/j.arth.2024.01.034

10. Dulieu-Barton JM (1999) Introduction to thermoelastic stress analysis. Strain 35:35–39. https://doi.org/10.1111/j.1475-1305.1999.tb01123.x

11. Hyodo K, Inomoto M, Ma W, Miyakawa S, Tateishi T (2001) Thermoelastic femoral stress imaging for experimental evaluation of hip prosthesis design. JSME Int J Ser C 44:1065–1071. https://doi.org/10.1299/jsmec.44.1065

12. Watanabe R, Mishima H, Yasunaga S, Yoshizawa T, Nishino T, Harada Y (2026) Femoral stress distribution in fully hydroxyapatite-coated cementless versus polished cemented stems with identical geometry: a thermoelastic stress analysis. Arch Orthop Trauma Surg 146:21. https://doi.org/10.1007/s00402-025-06165-4

13. Yasunaga S, Watanabe R, Nishino T, Yoshizawa T, Hirose F, Shimasaki K, Mishima H, Harada Y (2026) Influence of bone quality on femoral stress distribution after cemented stem insertion: an experimental thermoelastic stress analysis. Hip Int 36:541–549. https://doi.org/10.1177/11207000261420734

14. Cristofolini L, Viceconti M, Cappello A, Toni A (1996) Mechanical validation of whole bone composite femur models. J Biomech 29:525–535. https://doi.org/10.1016/0021-9290(95)00084-4

15. Heiner AD (2008) Structural properties of fourth-generation composite femurs and tibias. J Biomech 41:3282–3284. https://doi.org/10.1016/j.jbiomech.2008.08.013

16. Gluek C, Zdero R, Quenneville CE (2020) Evaluating the mechanical response of novel synthetic femurs for representing osteoporotic bone. J Biomech 111:110018. https://doi.org/10.1016/j.jbiomech.2020.110018

17. Cassar-Gheiti AJ, McColgan R, Kelly M, Cassar-Gheiti TM, Kenny P, Murphy CG (2020) Current concepts and outcomes in cemented femoral stem design and cementation techniques: the argument for a new classification system. EFORT Open Rev 5:241–252. https://doi.org/10.1302/2058-5241.5.190034

18. Thomson W (1851) On the dynamical theory of heat, with numerical results deduced from Mr Joule's equivalent of a thermal unit, and M Regnault's observations on steam. Trans R Soc Edinb 20:261–288.

19. Bergmann G, Deuretzbacher G, Heller M, Graichen F, Rohlmann A, Strauss J, Duda GN (2001)

428 Hip contact forces and gait patterns from routine activities. J Biomech 34:859–871.
429 https://doi.org/10.1016/S0021-9290(01)00040-9
430 20. Ministry of Health, Labour and Welfare of Japan (2026) National Health and Nutrition Survey
431 2024. https://www.mhlw.go.jp/content/001675217.pdf. Accessed 1 Jul 2026
432 21. Gruen TA, McNeice GM, Amstutz HC (1979) “Modes of failure” of cemented stem-type femoral
433 components: a radiographic analysis of loosening. Clin Orthop Relat Res 141:17–27.
434 22. Hashimoto K, Nakamura Y, Takahashi N, Morishima T (2026) Stem design and sizing influence
435 torsional periprosthetic fracture resistance of cemented stems in osteoporotic femoral models: a
436 comparative biomechanical study. Arthroplasty 8:53. https://doi.org/10.1186/s42836-026-00416-4
437 23. Mann KA, Bartel DL, Ayers DC (1997) Influence of stem geometry on mechanics of cemented
438 femoral hip components with a proximal bond. J Orthop Res 15:700–706.
439 https://doi.org/10.1002/jor.1100150511
440 24. Miyamoto S, Iida S, Suzuki C, Kawamoto T, Shinada Y, Ohtori S (2022) Minimum 10-year
441 follow-up of total hip arthroplasty with a collarless triple-tapered polished cemented stem with line-to-line
442 implantation using a direct anterior approach. J Arthroplasty 37:2214–2224.
443 https://doi.org/10.1016/j.arth.2022.05.022
444 25. Leclerc JT, Michou L, Vaillancourt F, Pelet S, Simonyan D, Belzile EL (2019) Prevalence and
445 characteristics of atypical periprosthetic femoral fractures. J Bone Miner Res 34:83–92.
446 https://doi.org/10.1002/jbmr.3584

26. Collins L, Nguyen HH, Milat F, Ebeling PR (2025) Epidemiology, pathophysiology and management of atypical femur fractures: an update. Curr Osteoporos Rep 23:40. https://doi.org/10.1007/s11914-025-00932-3

27. Baba T, Uchino M, Ochi H, Ikuta T, Saita Y, Hagino H, Nonomiya H, Jingushi S, Nakajima T, Ueda Y, Kaneko K (2021) Atypical periprosthetic femoral fractures after arthroplasty for fracture are at high risk of complications. Sci Rep 11:14378. https://doi.org/10.1038/s41598-021-93574-1

28. Tashiro K, Baba T, Fujita H, Iwase H, Ohashi H, Oe K, Otsuka M, Iwai S, Nakamura S, Morimoto T, Sawaguchi T, Nagai Y, Otsuki Y, Kim Y, Ishijima M (2026) Atypical periprosthetic femoral fractures around cemented stems: radiographic features and clinical implications from a multicenter study. Bone 204:117741. https://doi.org/10.1016/j.bone.2025.117741

29. Oh Y, Fujita K, Wakabayashi Y, Kurosa Y, Okawa A (2017) Location of atypical femoral fracture can be determined by tensile stress distribution influenced by femoral bowing and neck-shaft angle: a CT-based nonlinear finite element analysis model for the assessment of femoral shaft loading stress. Injury 48:2736–2743. https://doi.org/10.1016/j.injury.2017.09.023

30. Baryeh K, Mendis J, Sochart DH (2021) Temporal subsidence patterns of cemented polished taper-slip stems: a systematic review. EFORT Open Rev 6:331–342. https://doi.org/10.1302/2058-5241.6.200086